Aerodynamics of Heat Exchange Systems

Mark Drela 27 April 2016

1 Heat Load

The *heat load* $\dot{H}$ is the rate of thermal energy which is to be rejected from the system, typically to regulate the system's temperature. Example systems and their heat load sources are listed below.

System	Heat load origin
IC engine	heat conduction to engine mass, mechanical friction
Electric motor	resistive heating, mechanical friction, air friction
Electronics	resistive heating
Cabin interior	human metabolic heat generation
Heat exchanger	heat transport in via exchange fluid

For heat-cycle systems such as the IC engine, the heat load can typically be estimated from the known total energy input rate, minus the useful power output P, minus any external heat rejection rate which is not being considered. Specifically, we have

$$\dot{H} = \dot{m}_{\text{fuel}}\, h - P - \dot{H}_{\text{exh}} \tag{1}$$

$$= (h\, BSFC - 1)\, P - \dot{H}_{\text{exh}} \qquad \text{(IC engine)} \tag{2}$$

$$\dot{H}_{\text{exh}} \simeq \dot{m}_{\text{air}}\, c_p\, (T_{\text{exh}} - T_\infty) \tag{3}$$

where h is the fuel heating value, and $\dot{H}_{\text{exh}}$ is the heat rejection rate in the exhaust. The latter is given by the air mass flow rate and its temperature rise. For IC engines, the $\dot{H}$, P, and $\dot{H}_{\text{exh}}$ terms tend to be comparable in magnitude, so that assuming $\dot{H} \simeq P$ is a reasonable first estimate.

For electric motors, the heat load is the difference between the input electrical power and output shaft power,

$$\dot{H} = \dot{E}_{\text{elec}} - P \tag{4}$$

$$= \left(\frac{1}{\eta_{\text{m}}} - 1\right) P \qquad \text{(electric motor)} \tag{5}$$

where $\eta_{\text{m}} \equiv P/\dot{E}_{\text{elec}}$ is the motor efficiency. For electronic components which do not radiate EM waves, the heat load is simply the input electrical power.

$$\dot{H} = \dot{E}_{\text{elec}} \qquad \text{(electronics)} \tag{6}$$

2 Heat Rejection to Airflow

On an airborne vehicle in thermal steady state, the sum of all onboard heat loads must be rejected to the atmosphere, in the form of a heat transfer rate $\dot{Q}$ from the body to the airflow. Aircraft thermal equilibrium then requires this to be equal to the internal heat load.

$$\dot{Q} = \dot{H} \qquad \text{(in thermal equilibrium)} \tag{7}$$

At the high Reynolds numbers typical of aircraft, this heat transfer must occur through the boundary layers on the heat-rejecting radiator surfaces, as diagrammed in Figure 1. In low speed flow this can be calculated by

$$\dot{Q} = \iint \dot{q}_{\text{w}}\, \mathrm{d}S_r \tag{8}$$

$$\dot{q}_{\text{w}} = \rho_{\text{e}} u_{\text{e}}\, c_p (T_{\text{w}} - T_{\text{e}})\, c_h \tag{9}$$

in which the local *wall heat flux* $\dot{q}_\mathrm{w}$ is integrated over the radiator surface area S_r. The expression for $\dot{q}_\mathrm{w}$ is in terms of the flow conditions $\rho_\mathrm{e}, u_\mathrm{e}, T_\mathrm{e}$ just outside the edge of the boundary layer, the wall temperature T_w, and the *Stanton number* c_h.

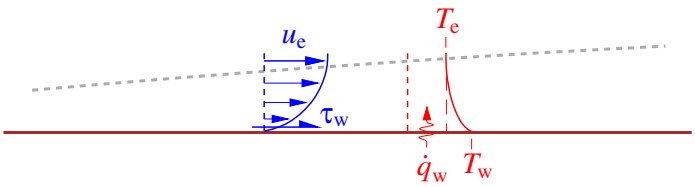

Figure 1: Convective heat transfer through surface boundary layer. Local wall heat flux $\dot{q}_\mathrm{w}$ and wall shear stress τ_w are related via Reynolds analogy.

Equation (9) is analogous to the expression for the wall shear stress in terms of the skin friction coefficient c_f.

$$\tau_\mathrm{w} \;=\; \tfrac{1}{2}\rho_\mathrm{e} u_\mathrm{e}^2\, c_f \tag{10}$$

For fluids with a near-unity Prandtl number, such as air with $Pr = 0.72$, and for near-flat plate flows, the Stanton number is related to the skin friction coefficient by

$$c_h \;=\; Pr^{-2/3}\,\tfrac{1}{2} c_f \tag{11}$$

which is called the *Reynolds analogy* [1]. We next apply the relations above to different types of radiator installations.

3 Skin radiator

A *skin radiator* is some portion of the aircraft's existing external surface whose temperature is raised using the heat from the heat load source. In low speed flow we can assume $\rho_\mathrm{e} \simeq \rho_\infty$, $T_\mathrm{e} \simeq T_\infty$, and for the typical skin radiator we can also assume $u_\mathrm{e} \simeq V_\infty$. In this case c_h, c_f become the flat-plate coefficients C_h, C_f normalized by V_∞, and we can also define the average skin friction coefficient.

$$\bar{C}_f \;\equiv\; \frac{1}{S_r}\iint C_f \,\mathrm{d}S_r \tag{12}$$

The overall heat flow (8) can now be written as

$$\boxed{\dot{Q} \;=\; \rho_\infty V_\infty\, c_p (T_\mathrm{w} - T_\infty) Pr^{-2/3} S_r\, \tfrac{1}{2}\bar{C}_f} \tag{13}$$

which is useful for estimating the heat rejection rate from a skin radiator since numerical values for $\bar{C}_{f(Re_\ell, Re_{x_\mathrm{tr}})}$ can be obtained from skin friction charts [1], as a function of the streamwise-length Reynolds number Re_ℓ, and also of the transition-length Reynolds number Re_{x_tr},

It is also useful to relate $\dot{Q}$ to the profile drag of the aircraft or aircraft component in question. Using the definition of the form factor K_f, we can write the profile drag as

$$D_p \;=\; \tfrac{1}{2}\rho_\infty V_\infty^2\, S_\mathrm{wet}\, \bar{C}_f\, K_f \tag{14}$$

where S_wet is the aircraft's or component's wetted area. Assuming $\bar{C}_f$ for the surface is comparable to that on the skin radiator, we can divide equations (13) and V_∞ times (14) to give

$$\frac{\dot{Q}}{D_p V_\infty} \;=\; \frac{1}{\gamma - 1}\,\frac{1}{M_\infty^2}\,\Delta\mathcal{T}\, Pr^{-2/3}\,\frac{S_r}{K_f S_\mathrm{wet}} \tag{15}$$

$$\Delta\mathcal{T} \;\equiv\; \frac{T_\mathrm{w} - T_\infty}{T_\infty} \tag{16}$$

where $\Delta\mathcal{T}$ is the *wall overheat ratio*, and the speed of sound relation $a^2 = (\gamma-1)c_pT$ was used.

Although skin radiators are attractive because of their potentially low added *cooling drag*, they have limited ability to reject the heat load of an IC engine, where heat flow considerably exceeds the total aircraft profile drag power D_pV_∞, so that both sides of equation (15) must be greater than unity. As a result, equation (15) can be difficult to satisfy with a practical amount of skin radiator area, except perhaps for very low speed aircraft where we have $M_\infty^2 \ll 1$.

4 Internal radiator

A fin radiator, or simply cooling fins attached to the heat-load source, has a relatively large amount of heat-transferring surface area in a relatively compact volume. To keep its cooling drag acceptably low, it is almost invariably enclosed in a cowl or diffusing duct to reduce the air velocity over the radiator, as diagrammed in Figure 2 [2].

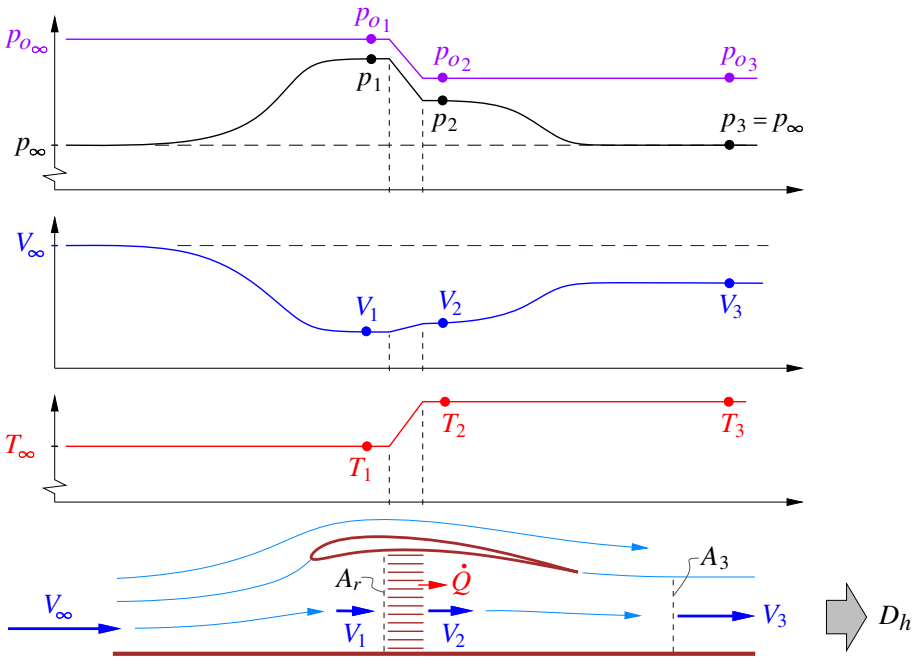

Figure 2: Cowled radiator installation, with streamwise distributions of temperature, velocity, and pressure. The cooling-flow temperature change $T_{o_3}-T_{o_\infty}$ and velocity change $V_\infty-V_3$ quantify the overall heat transfer $\dot{Q}$ and cooling drag D_h of the radiator installation.

The cowling surrounding the radiator decelerates the captured streamtube from V_∞ to V_1 just in front of the radiator. In this process there will also be an isentropic temperature rise from T_∞ to T_1, although for low speed flow we can assume $T_1 \simeq T_{o_\infty} \simeq T_\infty$, and also $\rho_1 \simeq \rho_\infty$. For a low-speed exhaust stream we can also assume $T_{o_3} \simeq T_3 \simeq T_2$. The cooling mass flow is

$$\dot{m}_r \;=\; \rho_1 V_1 A_r \;=\; \rho_2 V_2 A_r \;=\; \rho_3 V_3 A_3 \tag{17}$$

where A_r is the radiator frontal area and A_3 is the effective outflow area. Control volume analyses for the entire installation give the radiator heat transfer rate and overall cooling drag in terms of the total temperature and velocity flow changes from upstream to station 3.

$$\dot{Q} \;=\; \dot{m}_r\, c_p(T_{o_3}-T_{o_\infty}) \;\simeq\; \rho_1 V_1 A_r\, c_p(T_2-T_1) \tag{18}$$

$$D_h \;=\; \dot{m}_r\,(V_\infty - V_3) \;=\; \rho_1 V_1 A_r\,(V_\infty - V_3) \tag{19}$$

This D_h excludes any added profile drag on the outside surface of the cowl, which presumably would be analyzed separately by standard drag estimation techniques.

4.1 Cowled radiator heat transfer characterization

The heat transfer from the radiator could in principle be estimated by applying equations (8) and (9) to the radiator-vane surfaces. However, we note that for a radiator with a large internal surface area, the airflow will tend towards thermal equilibrium with the radiator, and specifically, T_2 will tend to approach T_r. It is therefore natural to define a heat-transfer effectiveness factor

$$\eta_h \;\equiv\; \frac{\dot{Q}}{\rho_1 V_1 A_r\, c_p (T_r - T_1)} \;=\; \frac{T_2 - T_1}{T_r - T_1} \;\le\; 1 \tag{20}$$

which can be measured experimentally for the radiator geometry in question [3]. As sketched in Figure 3, a lower Reynolds number (e.g. due to lower flow speed) gives thicker boundary layers and a higher effectiveness. We therefore expect the effectiveness to be a function $\eta_{h(Re_h)}$, where

$$Re_h \;\equiv\; \frac{1}{2}\left(\frac{\rho_1 V_1}{\mu_1} + \frac{\rho_2 V_2}{\mu_2}\right) \ell_h \tag{21}$$

is the average local Reynolds number over the radiator vane passage length ℓ_h. Once this function is obtained from measurements, the heat transfer from (18) is given by

$$\boxed{\dot{Q} \;=\; \rho_\infty V_\infty A_r\, c_p T_\infty \,\frac{V_1}{V_\infty}\, \Delta\mathcal{T}\, \eta_{h(Re_h)}} \tag{22}$$

where here the overheat ratio is defined from the radiator temperature, and also conveniently gives the exit/inlet temperature ratio.

$$\Delta\mathcal{T} \;\equiv\; \frac{T_r - T_1}{T_1} \;\simeq\; \frac{T_r - T_\infty}{T_\infty} \tag{23}$$

$$\frac{T_2}{T_1} \;\simeq\; \frac{T_2}{T_\infty} \;=\; 1 \,+\, \Delta\mathcal{T}\, \eta_h \tag{24}$$

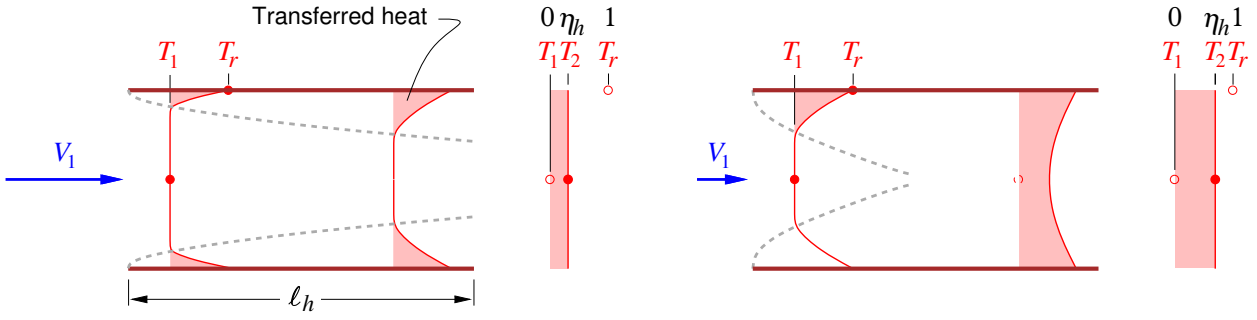

Figure 3: Temperature profiles across flow between two radiator fins. Radiator effectiveness η_h is the fraction that the final exit temperature T_2 moves from inlet T_1 to radiator T_r. Thicker merging boundary layers (on right) give larger effectiveness η_h, at a cost of excessive total pressure loss.

At first glance, it appears that $\eta_h \simeq 1$ is desirable in equation (22) to obtain the maximum heat transfer for the available radiator temperature and air mass flow. However, a high effectiveness in general implies that fully-developed flow has occurred for some distance along the radiator passages,

as sketched on right of Figure 3. This is undesirable since fully developed flow rapidly accumulates total pressure loss, while the local heat transfer rate decreases because the wall temperature gradient decreases. Hence, more modest effectiveness values, say $0.2 \leq \eta_h \leq 0.5$, will result in less cooling drag for a given amount of heat transfer.

4.2 Cowled radiator pressure drop characterization

The radiator pressure drop $p_1 - p_2$ can be estimated via a control volume analysis of the radiator core alone. This gives

$$p_1 + \rho_1 V_1^2 \; - \; p_2 - \rho_2 V_2^2 \;\; = \;\; f_r \tag{25}$$

where f_r is the average streamwise force per frontal area on the radiator, which is the net result of pressure and friction drag forces on the individual vanes. Since calculation of these forces on complex passage geometries is impractical, we capture their overall effect by defining the radiator pressure drop parameter [3].

$$\mathcal{P}_f \;\; \equiv \;\; \frac{f_r}{\frac{1}{2}\rho_1 V_1^2} \tag{26}$$

This can be measured for a range of flow conditions, which provides the function $\mathcal{P}_{f(Re_h)}$ for that radiator geometry. Typical values for liquid-air radiators fall in the range $5 < \mathcal{P}_f < 20$, with relatively "porous" or low-blockage radiators having the smaller values. With $\mathcal{P}_{f(Re_h)}$ known, the radiator pressure drop for any operating condition can be obtained from

$$p_1 - p_2 \;\; = \;\; \tfrac{1}{2}\,\rho_1 V_1^2\, \mathcal{P}_{f(Re_h)} \; + \; \rho_2 V_2^2 \; - \; \rho_1 V_1^2 \tag{27}$$

which depends not only on the inflow velocity V_1, but also on the heat transfer since this influences the station 2 conditions.

The typical expected form of the $\eta_{h(Re_h)}$ and $\mathcal{P}_{f(Re_h)}$ functions is diagrammed in Figure 4. The ideal operating point is close to the entrance/merged changeover, where the effectiveness is reasonably high, but the strong additional losses of fully-developed Poiseuille flow have not yet appeared.

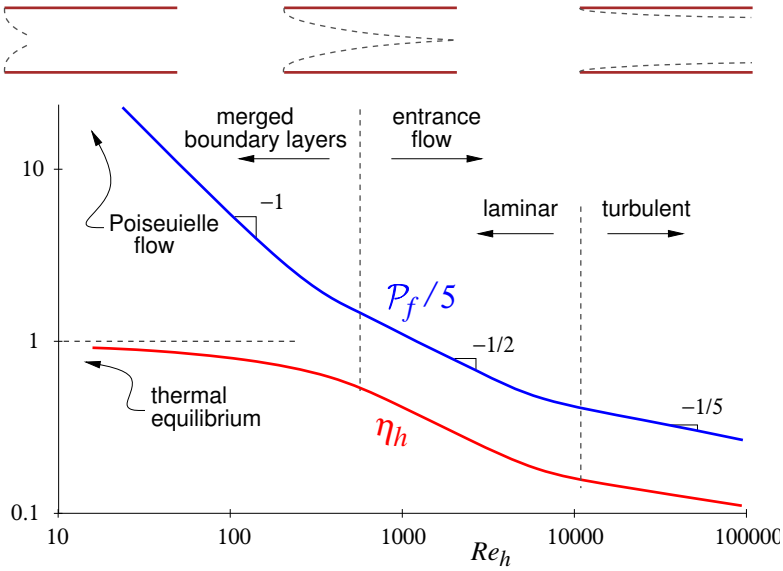

Figure 4: General behavior of $\eta_{h(Re_h)}$ and $\mathcal{P}_{f(Re_h)}$ functions.

4.3 Design characteristics

For cooling system *design*, the radiator frontal area A_r required for a specified heat transfer rate $\dot{Q}$ and a chosen V_1/V_∞ is obtained from (22).

$$\boxed{A_r \;=\; \frac{\dot{Q}}{\rho_\infty V_\infty \, c_p T_\infty} \, \frac{1}{\Delta\mathcal{T}\,\eta_h} \, \frac{1}{V_1/V_\infty}} \qquad \text{(design)} \qquad (28)$$

The cooling drag coefficient corresponding to this same $\dot{Q}$ and V_1/V_∞ is then obtained from (19),

$$C_{D_h} \;\equiv\; \frac{D_h}{\frac{1}{2}\rho_\infty V_\infty^2 \, S_{\rm ref}} \;=\; \frac{2\dot{Q}}{\rho_1 V_1 \, c_p (T_r - T_1) \eta_h \, S_{\rm ref}} \left(1 - \frac{V_3}{V_\infty}\right) \qquad (29)$$

where $S_{\rm ref}$ is the associated reference area. This can be further manipulated to the following form.

$$\boxed{C_{D_h} \;=\; \frac{\dot{Q}}{\frac{1}{2}\rho_\infty V_\infty^3 S_{\rm ref}} \, \frac{(\gamma-1)M_\infty^2}{\Delta\mathcal{T}\eta_h} \, \frac{1}{V_1/V_\infty} \left(1 - \frac{V_3}{V_\infty}\right)} \qquad \text{(design)} \qquad (30)$$

The expression for V_3/V_∞ will be derived later, with the final result given by (39).

Figure 5 shows typical variation of C_{D_h} at fixed $\dot{Q}$, versus V_1/V_∞ and $\Delta\mathcal{T}\,\eta_h$, as given by (30) together with (39). Here, $\mathcal{P}_f$ is kept proportional to $\Delta\mathcal{T}\eta_h$ as suggested by Figure 4, which reflects the fact that radiators with greater effectiveness will typically also have greater pressure losses.

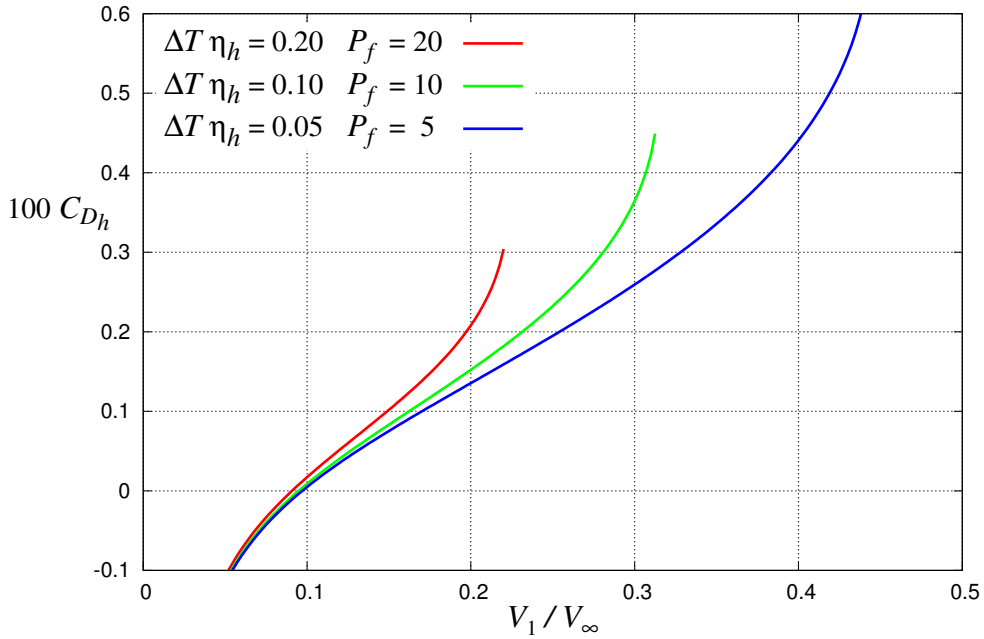

Figure 5: Typical cooling drag coefficient dependence on the inflow velocity ratio for the design sizing case, for three different net overheat ratios $\Delta\mathcal{T}\,\eta_h$, and proportionally-varied pressure loss parameters $\mathcal{P}_f$.

The negative C_{D_h} values for small V_1/V_∞ are due to the radiator installation acting as a ramjet [4], [5], as captured by the $1 + \Delta\mathcal{T}\,\eta_h$ coefficient in the V_3/V_∞ expression (39). However, the required small V_1/V_∞ values imply large and hence heavy radiator installations, which will also have considerable added external cowling drag which is not included in C_{D_h}. Hence, actually realizing a negative cooling drag is not necessarily the best solution from an overall aircraft system viewpoint.

4.4 Cooling system performance estimation

To estimate the radiator mass flow, and subsequently the heat transfer and cooling drag, we first apply the Bernoulli equation between far-upstream and station 1, $p_{o_\infty} = p_{o_1}$, or equivalently

$$p_\infty \,+\, \tfrac{1}{2}\rho_\infty V_\infty^2 \;=\; p_1 \,+\, \tfrac{1}{2}\rho_\infty V_1^2 \tag{31}$$

and also between stations 2 and 3, $p_{o_3} = p_{o_2}$, or equivalently

$$p_\infty \,+\, \tfrac{1}{2}\rho_2 V_3^2 \;=\; p_2 \,+\, \tfrac{1}{2}\rho_2 V_2^2 \tag{32}$$

where we made the low-speed approximations $\rho_1 \simeq \rho_\infty$ and $\rho_3 \simeq \rho_2$. Subtracting equation (31) from (32), and using the pressure-drop expression (27), gives

$$\tfrac{1}{2}\rho_2 V_3^2 \,-\, \tfrac{1}{2}\rho_\infty V_\infty^2 \;=\; -\tfrac{1}{2}\rho_\infty V_1^2\,\mathcal{P}_f \,-\, \tfrac{1}{2}\rho_2 V_2^2 \,+\, \tfrac{1}{2}\rho_\infty V_1^2 \tag{33}$$

in which V_2 and V_3 can be replaced with the mass flow relations (17),

$$V_2 \;=\; V_1\frac{\rho_1}{\rho_2} \;=\; V_1\frac{p_1}{p_2}\frac{T_2}{T_1} \;\simeq\; V_1\frac{T_2}{T_1} \tag{34}$$

$$V_3 \;=\; V_1\frac{\rho_1}{\rho_2}\frac{A_r}{A_3} \;\simeq\; V_1\frac{T_2}{T_1}\frac{A_r}{A_3} \tag{35}$$

where the low-speed ideal gas law and the low speed approximation $p_1/p_2 \simeq 1$ were also used. Also using (22) to eliminate T_2/T_1 in terms of $\dot{Q}$, equation (33) then becomes

$$\left[\frac{A_r^2}{A_3^2} \,+\, \mathcal{P}_f\right]\frac{V_1^2}{V_\infty^2} \,+\, \left[\left(\frac{A_r^2}{A_3^2}+1\right)\frac{\dot{Q}}{\rho_\infty V_\infty A_r\, c_p T_\infty}\right]\frac{V_1}{V_\infty} \;=\; 1 \tag{36}$$

which is a quadratic equation for the radiator velocity ratio V_1/V_∞ as a function of $\dot{Q}$ and A_3/A_r. Some iteration will be needed if $\mathcal{P}_f$ is assumed to be some known function of V_1. The resulting radiator temperature and exit velocity ratio then follow.

$$\begin{aligned}\frac{T_r}{T_\infty} \;&=\; 1+\Delta\mathcal{T} \\ &=\; 1 \,+\, \frac{\dot{Q}}{\rho_\infty V_\infty A_r\, c_p T_\infty}\frac{V_\infty}{V_1}\frac{1}{\eta_h(Re_h)} \end{aligned} \tag{37}$$

$$\begin{aligned}\frac{V_3}{V_\infty} \;&=\; \frac{V_1}{V_\infty}(1+\Delta\mathcal{T}\eta_h)\frac{A_r}{A_3} \\ &=\; \sqrt{\frac{T_2}{T_\infty}\left[1-\frac{V_1^2}{V_\infty^2}\mathcal{P}_f \,+\, \frac{V_1^2}{V_\infty^2}\left(1-\frac{T_2}{T_\infty}\right)\right]} \end{aligned} \tag{38}$$

Using (24) we can further substitute for T_2/T_∞ to reveal the explicit dependence on all the dimensionless parameters.

$$\boxed{\frac{V_3}{V_\infty} \;=\; \sqrt{(1+\Delta\mathcal{T}\eta_h)\left[1-\frac{V_1^2}{V_\infty^2}\mathcal{P}_f \,-\, \frac{V_1^2}{V_\infty^2}\Delta\mathcal{T}\eta_h\right]}} \qquad \text{(operation)} \tag{39}$$

Using this result, the cooling drag coefficient can then be obtained from (19),

$$\boxed{C_{D_h} \;\equiv\; \frac{D_h}{\frac{1}{2}\rho_\infty V_\infty^2\, S_{\text{ref}}} \;=\; 2\frac{A_r}{S_{\text{ref}}}\frac{V_1}{V_\infty}\left(1-\frac{V_3}{V_\infty}\right)} \qquad \text{(operation)} \tag{40}$$

where S_{ref} is the associated reference area.

4.5 Operational characteristics

Equation (40) is the "operation" cooling drag coefficient in that it corresponds to the operation of a given radiator installation, whose V_1/V_∞ ratio can be regulated by varying the cowl exit area. Typical results are shown in Figure 6, together with the operating heat transfer given by (13). In practice, V_1/V_∞ would be set by the need to maintain some tolerable temperature of the heat load source, and there will be some corresponding cooling drag as a result.

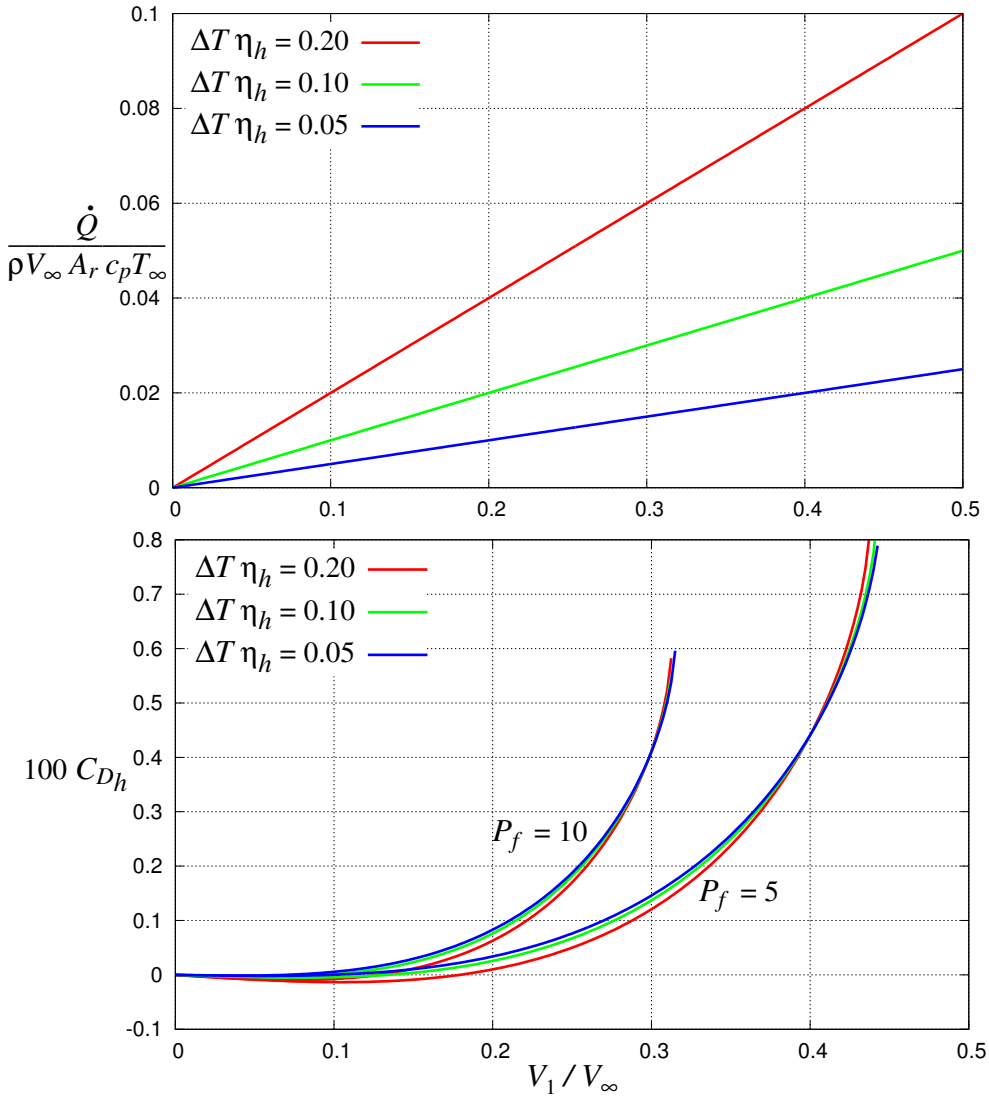

Figure 6: Typical heat transfer and cooling drag dependence on the inflow velocity ratio for fixed radiators with two different pressure drop parameters $\mathcal{P}_f$. Larger $\Delta\mathcal{T}\eta_h$ would be due to a larger radiator temperature T_r.

References

[1] H. Schlichting. *Boundary-Layer Theory.* McGraw-Hill, New York, 1979.

[2] S.F. Hoerner. *Fluid-Dynamic Drag.* Hoerner Fluid Dynamics, Vancouver, WA, 1965.

[3] W.M. Kays and A.L. London. *Compact Heat Exchangers.* McGraw-Hill, New York, 1984.

[4] P. Rauscher and W.H. Phillips. Propulsive effects of radiator and exhaust ducting. *Journal of the Aeronautical Sciences*, 8(11):167–174, Nov 1940.

[5] M. Drela. Aerodynamics of heat exchangers for high-altitude aircraft. *Journal of Aircraft*, 33(2), Mar-Apr 1996.